





## Article

# Recoverable and Sensitive Pressure-Induced Mechanochromic Photoluminescence of a Au-P Complex

Ningwen Yang<sup>1</sup>, Yijia Chang<sup>1</sup>, Jiangyue Wang<sup>1</sup>, David James Young<sup>2</sup> , Hong-Xi Li<sup>1</sup> , Yuxin Lu<sup>1,\*</sup>  and Zhi-Gang Ren<sup>1,\*</sup> 

<sup>1</sup> College of Chemistry, Chemical Engineering and Materials Science, Soochow University, Suzhou 215123, China

<sup>2</sup> James Watt School of Engineering, University of Glasgow, University Avenue, Glasgow G12 8QQ, UK

\* Correspondence: luyuxin@suda.edu.cn (Y.L.); renzhigang@suda.edu.cn (Z.-G.R.)

**Abstract:** A binuclear Au-P complex [Au<sub>2</sub>(2-bdppmapy)<sub>2</sub>](PF<sub>6</sub>)<sub>2</sub> (**1**) was synthesised by the reaction of 2-bdppmapy (N,N'-bis-(diphenylphosphanylmethyl)-2-aminopyridine) with AuCN and [Cu(MeCN)<sub>4</sub>]PF<sub>6</sub>. The solid phase of **1** emitted bright yellow phosphorescence at λ<sub>max</sub> = 580 nm under UV excitation (QY = 4.41%, τ = 1.88 μs), which shifted to green (λ<sub>max</sub> = 551 nm, QY = 5.73%) after being pressurised under 5 MPa. This colour change was recoverable upon exposure to CH<sub>2</sub>Cl<sub>2</sub> vapor. Similar mechanochromic photoluminescence behaviour was observed after grinding the crystals of **1**. A filter paper impregnated with **1** demonstrated recyclable write/erase functionality for encrypted information transfer.

**Keywords:** Ag-P complex; stimuli-responsive material; mechanochromic photoluminescence; photoluminescent material

## 1. Introduction

Stimuli-responsive complexes with tuneable photoluminescence (PL) have gained considerable attention in recent years [1–5] due to their potential applications as sensors [6–8], PL switches [9–11], and data storage devices [12–14]. Upon exposure to external stimuli, these complexes exhibited visible colour changes in emission, which can be induced by light [15–17], electrical current [18–20], heat [21–24], solvent [25–27], and mechanical force [28–36]. Mechanochromic photoluminescence, a phenomenon where mechanical force alters the emission colour [37–39], has been attributed to changes in molecular arrangement [29,40,41], conformational flexibility [42,43], or altered intermolecular interactions [44–46]. A number of gold, silver, and platinum complexes emit bright PL in the solid state, and their emission energies can be tuned by variations in metal–ligand coordination bonds, metal–metal interactions, and weak interactions such as van der Waals forces and hydrogen bonds [47–51]. Over the past decades, these complexes have emerged as attractive stimuli-responsive mechanochromic PL materials. For example, an anthryl Au(I) isocyanide complex demonstrated a bathochromic shift in emission from the visible to infrared region upon grinding, attributed to enhanced intermolecular aurophilic interactions [52].

The mechanochromic PL of complexes is most commonly induced by grinding. Under static high pressures (GPa-level), some Cu-N and Pt-N complexes exhibit chromic PL, which recovers to original colours when the pressures are released [53–55]. Determining the precise origin of mechanochromic PL is challenging due to the loss of crystallinity complicating solid-state structural characterisation, even though Ito and coworkers reported



Academic Editor: Takashiro Akitsu

Received: 22 March 2025

Revised: 29 April 2025

Accepted: 29 April 2025

Published: 30 April 2025

**Citation:** Yang, N.; Chang, Y.; Wang, J.; Young, D.J.; Li, H.-X.; Lu, Y.; Ren, Z.-G. Recoverable and Sensitive Pressure-Induced Mechanochromic Photoluminescence of a Au-P Complex. *Molecules* **2025**, *30*, 2011. <https://doi.org/10.3390/molecules30092011>

**Copyright:** © 2025 by the authors. Licensee MDPI, Basel, Switzerland. This article is an open access article distributed under the terms and conditions of the Creative Commons Attribution (CC BY) license (<https://creativecommons.org/licenses/by/4.0/>).

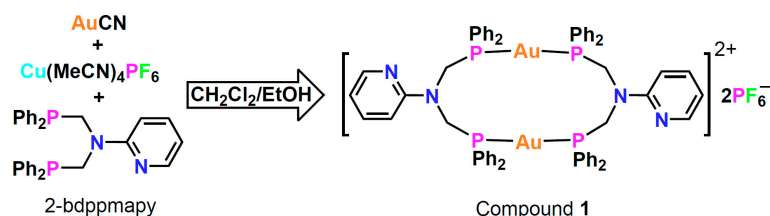
novel mechano-force-triggered luminescence in Au complexes arising from single-crystal-to-single-crystal domino transformations, while a minor mechano-stimulus is required to trigger the PL [34,35,56].

Various Au(I) complexes with phosphine ligands have exhibited stimuli-responsive PL toward vapor, ions, solvent, and mechano-forces [57–60], and this has encouraged us to explore the PL behaviours of Au(I) with some hybrid phosphine ligands containing  $-PPh_2$  groups and other donors such as  $-Py$ ,  $-phen$ ,  $-Pz$ ,  $C=S$ , and  $-C\equiv CH$  groups [61–63], as the secondary donor group may supply additional sites for coordination and non-covalent interactions that activating the changing over PL. For example, we recently reported that a Au-P-S complex exhibited switchable PL upon grinding, related to the collapse and restoration of the crystalline phase accompanied by the disruption and reforming of intermolecular hydrogen bonds. However, this PL did not change after being treated under static pressure up to 12 MPa [62]. In the current work, we carried out the reaction of the PNP-type ligand 2-bdppmapy (N,N-bis-(diphenylphosphanylmethyl)-2-aminopyridine) with AuCN and  $[Cu(MeCN)_4]PF_6$ , intended to generate some heterometallic Au/Cu complexes with good PL responses. Unexpectedly, this reaction lead to the formation of a new complex  $[Au_2(2-bdppmapy)_2](PF_6)_2$  (**1**), which contains only two Au(I) metal centres in the structure. The PL of **1** in the solid state changes from yellow to green induced by static pressures as low as 2.5 MPa and can be recovered by exposure to  $CH_2Cl_2$  vapor, making it suitable for encrypted information transfer.

## 2. Results and Discussion

### 2.1. Synthesis and Characterisation

Crystals of **1**·EtOH were isolated from the reaction of 2-bdppmapy, AuCN, and  $[Cu(MeCN)_4]PF_6$  (molar ratio 1:1:1) in  $CH_2Cl_2$ /EtOH at room temperature followed by the diffusion of petroleum ether and  $Et_2O$  into the reaction mixture (Scheme 1). The driving force for this metathesis was the precipitation of insoluble CuCN. Changing the ratios and salts did not improve the yield.



**Scheme 1.** Synthesis of compound **1**.

The EtOH solvent molecules were eliminated quickly from the crystal of **1**·EtOH and resulted in solventless **1** in 58% yield. Compound **1** was stable in air and water, soluble in MeCN, DMF, and DMSO, partially soluble in  $CH_2Cl_2$ ,  $CHCl_3$ , MeOH, and EtOH, and insoluble in other common solvents. Elemental analysis of **1** was consistent with its chemical formula. The TGA curve of **1** (Figure S1) revealed that it had no EtOH solvent molecules at room temperature. It was thermally stable below 250 °C, and subsequently lost its organic components at higher temperatures. The PXRD pattern of **1** generally matched that simulated from the single-crystal X-ray diffraction (SCXRD) data of **1**·EtOH, indicating the main cell parameters remained, whereas the intensity of some peaks varied due to the elimination of EtOH molecules (Figure S2). The IR spectrum of **1** (Figure S3) contained signals attributable to the stretching vibrations of the  $-Ph$  and  $-Py$  groups at 1591, 1475, 1435, 775, 733, and 691  $cm^{-1}$ ; of the  $-CH_2-$  group at 1475  $cm^{-1}$ ; and of the  $PF_6^-$  anion at 829  $cm^{-1}$ , while that of **1**·EtOH showed the peaks of the lattice EtOH molecule at 3344  $cm^{-1}$  ( $-OH$ ), 2976, and 2880  $cm^{-1}$  ( $-C_2H_5$ ). The  $^1H$  NMR spectrum of **1** in  $DMSO-d_6$

(Figure S4) consisted of signals assignable to the  $-\text{CH}_2-$  group (4.22 ppm) and the  $-\text{Py}$  and  $-\text{Ph}$  groups (8.06–6.57 ppm). The  $^{31}\text{P}\{\text{H}\}$  NMR spectrum contained a single resonance at 44.66 ppm.

SCXRD analysis of **1**·EtOH at 223 K revealed that it crystallised in the space group  $P2_1/n$ . Each asymmetric unit contains half of the  $[\text{Au}_2(2\text{-bdppmapy})_2]^{2+}$  dication, one  $\text{PF}_6^-$  anion, and half of the EtOH molecule. Two Au atoms and two 2-bdppmapy molecules are bonded head-to-head to form a distorted  $\text{Au}_2\text{P}_4$  quadrilateral structure (Figure 1). The Au1 atom is coordinated with two  $-\text{PPh}_2$  groups with the P–Au–P bond angle of  $174.37(8)^\circ$ . The mean Au–P bond length is  $2.309(2)$  Å. The distance between Au1 and Au1A ( $4.550$  Å) confirms the absence of an aurophilic interaction.

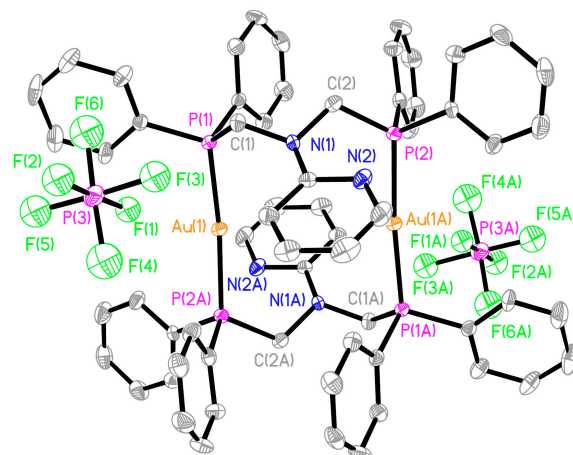


**Figure 1.** Crystal structure of **1**·EtOH with 30% thermal ellipsoids. All H atoms, disordered F atoms, and the EtOH solvent molecule are omitted for clarity. Symmetry code for A:  $1 - x, 1 - y, 1 - z$ .

## 2.2. Photophysical Properties

The PL responses of **1** in the solid state and in solution at room temperature were recorded (Figure 2). Upon excitation at  $\lambda_{\text{max}} = 345$  nm, a solid sample of **1** emitted yellow ( $\lambda_{\text{max}} = 580$  nm) with a quantum yield (QY) of 4.41%. The microsecond lifetime ( $\tau = 1.88$   $\mu\text{s}$ , excited at 370 nm, measured by transient PL) indicated phosphorescent emission. By comparison, solutions of **1** in MeCN, DMSO, and DMF were non-emissive, likely due to the interactions between **1** and these polar solvents, as well as free rotation of the  $-\text{Ph}$  groups in solutions that facilitate non-radiative relaxation of the excited state.

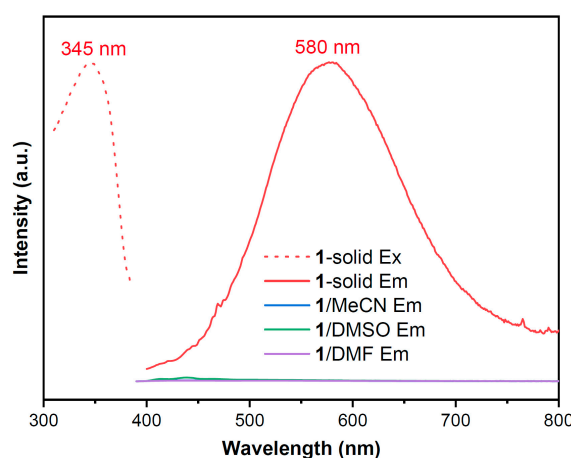


**Figure 2.** Excitation (dotted line) and emission (solid line) spectra of **1** in the solid state and in solution (1 mg/mL).

Density functional theory (DFT) calculations based on the SCXRD data of **1** were employed to calculate the frontier orbital distributions. As shown in Figure 3, the HOMOs were mainly located at the  $\pi$  orbitals of the –Py group. The LUMO was delocalised over the Au–P bond, while the LUMO+1 was mainly located at the  $\pi^*$  orbitals of the –Ph group. The PL of compound **1** is likely due to ligand-to-metal charge transfer ( $^3$ LMCT) combined with intra-ligand charge transfer ( $^3$ ILCT) [64,65].

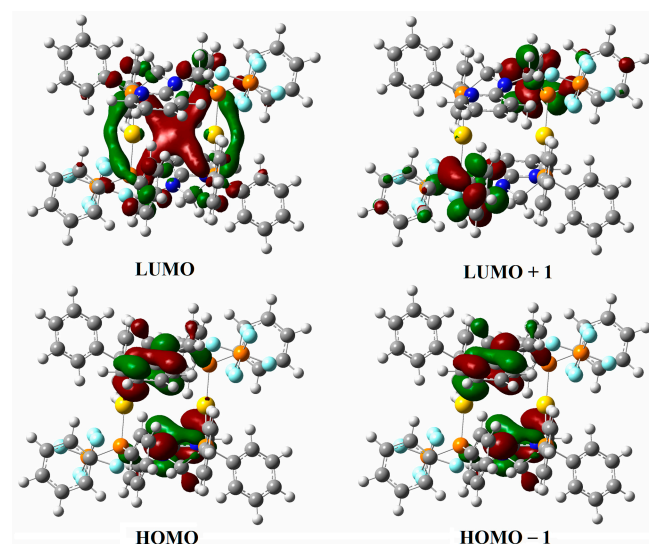


**Figure 3.** The orbital distributions of HOMOs and LUMOs (isovalue = 0.03) in compound **1**.

### 2.3. Pressure-Induced Mechanochromic Photoluminescence

We investigated the PL of five samples of **1** after exposure to different pressures (1–1 MPa, 1–2.5 MPa, 1–5 MPa, 1–10 MPa, 1–20 MPa) for 10 min (Figure 4a). The emission  $\lambda_{\max}$  of **1** remained unchanged in response to low pressure (1–1 MPa, 580 nm), but shifted to shorter wavelengths in response to higher pressures (1–2.5 MPa,  $\lambda_{\max}$  = 573 nm; 1–5 MPa,  $\lambda_{\max}$  = 551 nm; 1–10 MPa,  $\lambda_{\max}$  = 547 nm; and 1–20 MPa,  $\lambda_{\max}$  = 547 nm). Accompanied with a slightly enhanced QY (5.73% for 1–5 MPa), this yellow-to-green colour change was visible to the naked eye (Figure 4b,c).

PXRD patterns were obtained to examine the phase transition of **1** in response to pressure. In the PXRD patterns of 1–5 MPa, 1–10 MPa, and 1–20 MPa, the major peaks at  $2\theta$  = 8.3° (h, k, l = 0, 1, 1), 8.6° (h, k, l = 1, 0, 1), 9.8° (h, k, l = 1, 1, 0) vanished, while peaks at 8.5°, 8.8° and 9.9° appeared. The changing on PXRD peaks indicated the change in interplanar crystal spacing distances and the forming of a new crystalline phase. By comparison, the PXRD pattern of 1–2.5 MPa contained peaks corresponding to both phases, demonstrating incomplete phase-transition. In the case of 1–1 MPa, weak signals at 8.9° and 9.0° were also observable, illustrating that this phase transition could occur slightly even at low pressure.

Since the changes in the emission spectra and PXRD patterns were almost complete after 10 min at 5 MPa, we used this sample as a model. When 1–5 MPa was exposed to  $\text{CH}_2\text{Cl}_2$  vapor for 5 min, the resulting solid (**1r**) emitted at 582 nm, almost identical to the PL of **1**. Likewise, the PXRD pattern of **1r** showed peaks at  $2\theta$  = 8.4°, 8.7°, and 9.8°, again almost identical to **1** (Figure 4a,c). This cycle of pressure and exposure to  $\text{CH}_2\text{Cl}_2$  vapor was repeated five times without noticeable changes in the PL wavelengths of the two phases (Figure S5).

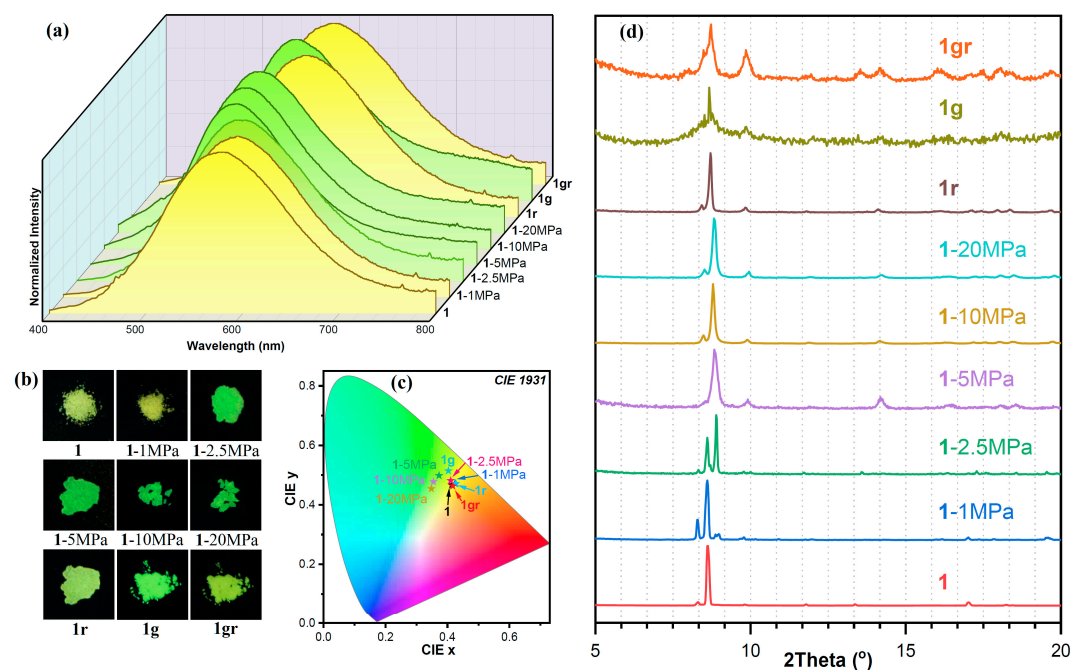


**Figure 4.** Comparisons of (a) emission spectra (excited at 354 nm), (b) photos under 365 nm LED irradiation, (c) CIE plot, (d) PXRD patterns of **1**, in response to different pressures for 10 min (**1**—1 MPa, **1**—2.5 MPa, **1**—5 MPa, **1**—10 MPa, **1**—20 MPa), **1r** (**1**—5 MPa after exposure to  $\text{CH}_2\text{Cl}_2$  vapor), **1g** (**1** ground in a mortar), and **1gr** (**1g** after exposure to  $\text{CH}_2\text{Cl}_2$  vapor).

When **1** was ground in a mortar, the emission of the resulted solid **1g** blue-shifted to  $\lambda_{\text{max}} = 557$  nm, in-between the wavelengths of **1**—2.5 MPa and **1**—5 MPa (Figure 4a), indicating that grinding had less of a mechanochromic PL effect than pressure at 5 MPa. When **1g** was exposed to  $\text{CH}_2\text{Cl}_2$  vapor, the emission of the resulted solid (**1gr**) also recovered to  $\lambda_{\text{max}} = 580$  nm. Although the PXRD patterns of **1g** and **1gr** were less crystalline, some peaks were observable. The PXRD pattern of **1g** showed peaks at  $2\theta = 8.5^\circ$ ,  $8.7^\circ$ , and  $9.9^\circ$ , which recovered to  $2\theta = 8.5^\circ$ ,  $8.7^\circ$ , and  $9.8^\circ$  in **1gr**. These emission spectra and PXRD patterns indicated that the phase transition induced by grinding was broadly similar to that induced by static pressure.

To explain these phase transitions, we investigated the SCXRD data and calculated that there was a total void of  $204.2 \text{ \AA}^3$  in each cell (Figure S6, 6.3% of cell volume, calculated using PLATON v1.18) in the crystal structure of **1**. We then performed nitrogen adsorption/desorption experiments which indicated that the pore volume of **1** ( $0.042 \text{ cm}^3/\text{g}$ ) was reduced to nearly half in **1**—5 MPa ( $0.021 \text{ cm}^3/\text{g}$ ), and was restored in **1r** ( $0.047 \text{ cm}^3/\text{g}$ ). We therefore concluded that pressure reduced the void in the crystal structure in **1**, and  $\text{CH}_2\text{Cl}_2$  molecules then inserted into the voids and restored the unit cell, which has been observed in other mechanochromic Au complexes [66–68]. Examination of the SCXRD data also indicated various C—H $\cdots$ F hydrogen bonds (Table 1 and Figure 5a) between the  $[\text{Au}_2(2\text{-bdppmapy})_2]^{2+}$  dication and the  $\text{PF}_6^-$  anions, and a number of intra- and inter-molecular C—H $\cdots$  $\pi$  interactions (Table 2 and Figure 5b) between neighbouring  $[\text{Au}_2(2\text{-bdppmapy})_2]^{2+}$  dications.

We examined the Hirshfeld surfaces to quantify the contribution of non-covalent interactions in the crystal packing. The software Multiwfn v3.8 [69] was used for the analysis of the Hirshfeld surface. As shown in the coloured map of  $d_{\text{norm}}$  (Figure 6), the red-coloured regions signified the presence of the aforementioned hydrogen bonds and C—H $\cdots$  $\pi$  interactions, which were consistent with the results obtained from PLATON calculations.



**Table 1.** Hydrogen bond lengths (Å) and angles (°) in **1** (calculated by PLATON v1.18).

D–H...A	D–H	H...A	D...A	D–H...A
C1–H1B...F3	0.98	2.42	3.35(2)	157
C2–H2A...F6 <sup>i</sup>	0.98	2.48	3.09(2)	120
C6–H6...F4 <sup>ii</sup>	0.94	2.43	3.21(2)	141
C21–H21...F2 <sup>i</sup>	0.94	2.51	3.34(2)	147

Symmetry codes: (i)  $0.5 - x, -0.5 + y, 1.5 - z$ ; (ii)  $-x, 1 - y, 1 - z$ .

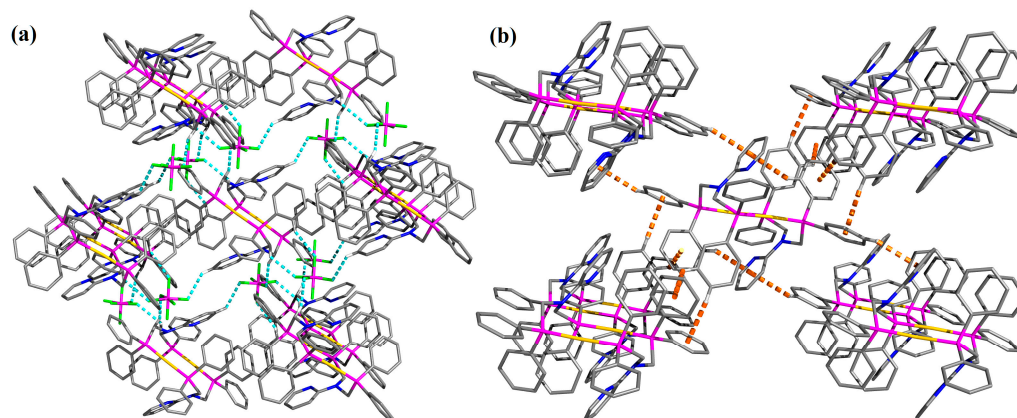


**Figure 5.** (a) Hydrogen bonds (dashed light-blue lines) between the [Au<sub>2</sub>(2-bdppmapy)<sub>2</sub>]<sup>2+</sup> dication and the PF<sub>6</sub><sup>−</sup> anions. All non-hydrogen-bonded H atoms are omitted for clarity; (b) C–H...π interactions (dashed yellow lines) between neighbouring [Au<sub>2</sub>(2-bdppmapy)<sub>2</sub>]<sup>2+</sup> dications. All hydrogen atoms and PF<sub>6</sub><sup>−</sup> anions are omitted for clarity. Atom colors: Au, light-yellow; P, magenta; N, blue; C, gray; F, green; H, white.

**Table 2.** C–H...π interaction distances (Å) and γ angles (°) in **1** (calculated by PLATON v1.18).

D–H...Cg	H...Cg	γ
C9–H9...Cg1 <sup>i</sup>	2.76	7.7
C17–H17...Cg1 <sup>ii</sup>	2.84	10.9
C22–H22...Cg2 <sup>iii</sup>	2.91	11.9
C23–H23...Cg3 <sup>iii</sup>	2.86	8.7

Cg1: N2, C3–C7; Cg2: C8–C13; Cg3: C14–C19; Symmetry codes: (i)  $1 - x, 1 - y, 1 - z$ ; (ii)  $0.5 - x, 0.5 + y, 1.5 - z$ ; (iii)  $1.5 - x, -0.5 + y, 1.5 - z$ .

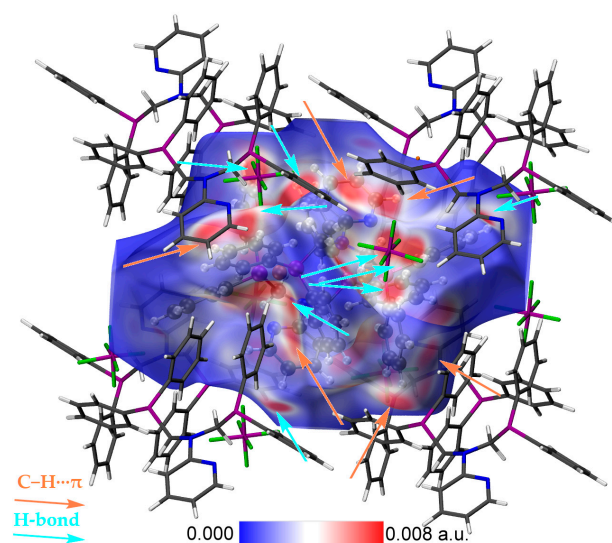


**Figure 6.** The Hirshfeld surface analysis of compound **1**. Light-blue and yellow arrows directed to the hydrogen bonds and C–H...π interactions, respectively.

Comparing the IR spectra of **1** and **1**—5 MPa (Figure 7), the characteristic absorption of  $\text{PF}_6^-$  at  $829\text{ cm}^{-1}$  remained unchanged. However, the signals for the  $-\text{Ph}$  and  $-\text{Py}$  groups at  $1506\text{ cm}^{-1}$  distinctly weakened in the latter, and some new weak signals at  $1558$ ,  $1541$ ,  $1520$ , and  $1506\text{ cm}^{-1}$  appeared. These IR spectral data suggest that during mechanical pressing, the hydrogen bonding environment of the  $\text{PF}_6^-$  anion was minimally affected, whereas the chemical environment around the  $-\text{Ph}$  and  $-\text{Py}$  groups was significantly affected. These spectral changes were restored in **1r**, consistent with the restoration of the emission spectra. To this end, we propose that pressure mostly disrupts the  $\text{C-H}\cdots\pi$  interactions associated with the  $-\text{PPh}_2$  and  $-\text{Py}$  groups, thereby altering the emission of **1** in the solid state.

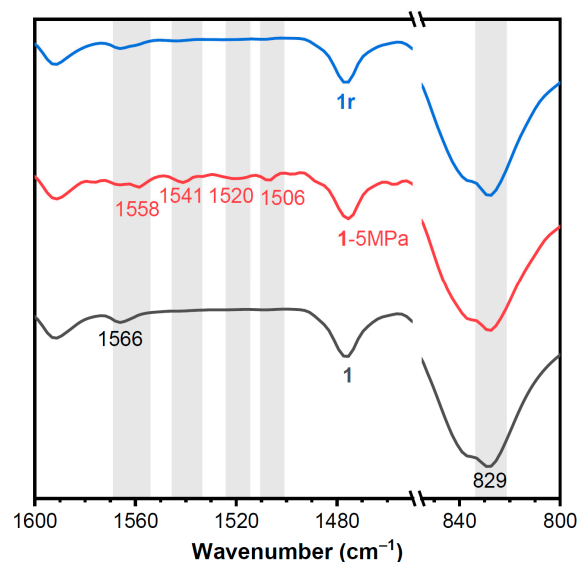


Figure 7. Comparison of the IR spectra of **1**, **1**—5 MPa, and **1r** in the range  $800\text{--}1600\text{ cm}^{-1}$ .

#### 2.4. Application to Encrypted Information Transfer

This responsiveness of the PL of complex **1** to external stimuli was used to make invisible ink [70]. Compound **1** was impregnated on filter paper and activated by  $\text{CH}_2\text{Cl}_2$  vapor. Writing on a thin cover paper placed over the filter paper using an inkless ball-point pen (Figure 8) at normal writing strength did not produce a noticeable change under natural light. However, writing appeared under UV light at  $365\text{ nm}$ , and could be erased by exposure to a  $\text{CH}_2\text{Cl}_2$  atmosphere for  $5\text{ min}$ . This write/erase operation could be repeated several times and endowed compound **1** as an encrypted information transformation material.

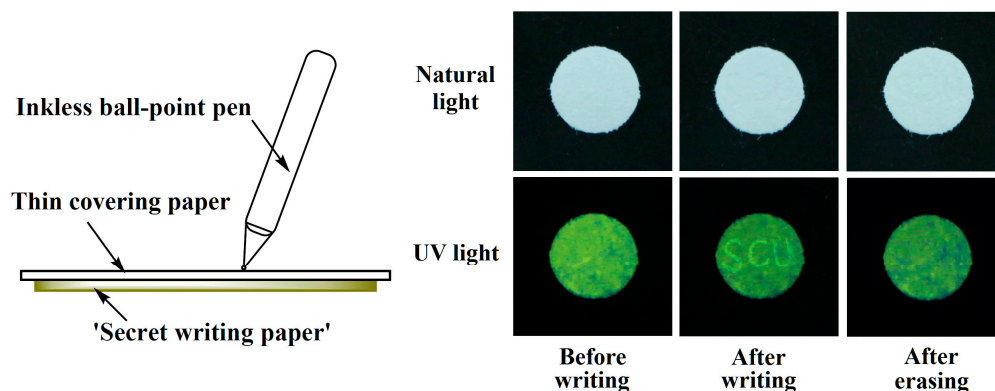


Figure 8. (left) Schematic plot of the encrypted information transfer experiment; (right) photos of the 'secret writing paper' under natural and UV ( $365\text{ nm}$ ) light before/after writing 'SCU' and erasing with  $\text{CH}_2\text{Cl}_2$  vapor.

### 3. Experimental Section

#### 3.1. Materials, Characterisation, and Measurements

2-Bdppmapy was prepared using a method from the literature [71]. All other materials were supplied from commercial sources and used as received. Elemental analyses were performed on a Thermal Fisher Flash Smart microanalyzer (Thermo Fisher Scientific, Waltham, MA, USA). Powder X-ray diffraction (PXRD) patterns were recorded on a Bruker D2 Phaser X-ray diffractometer (Bruker, Billerica, MA, USA) with the Bragg–Brentano method using a Cu K $\alpha$  source (30 kV, 10 mA). IR spectra were acquired on a Bruker VERTEX 70 FT-IR spectrometer (4000–600 cm<sup>−1</sup>) (Bruker, Billerica, MA, USA) with an ATR probe. Thermogravimetric analysis (TGA) was performed on a TA SDT-2960 analyser (TA Instruments, New Castle, DE, USA) from room temperature to 800 °C under a N<sub>2</sub> stream, with a heating rate of 10 °C /min. NMR spectra were acquired on a Bruker AVANCE NEO NMR spectrometer (Bruker, Billerica, MA, USA). N<sub>2</sub> adsorption/desorption experiments were conducted using a Belsorp-Max gas adsorption analyser (Microtrac BEL, Osaka, Japan). Emission spectra, transient photoluminescence, and QY measurements were performed on an Edinburgh FLS1000 spectrometer (Edinburgh Instruments, Livingston, UK).

#### 3.2. Synthesis of [Au<sub>2</sub>(2-Bdppmapy)<sub>2</sub>](PF<sub>6</sub>)<sub>2</sub> (**1**)

A mixture of CH<sub>2</sub>Cl<sub>2</sub>/EtOH (*v/v* = 1:1, 6.0 mL), AuCN (8.92 mg, 0.04 mmol), and 2-bdppmapy (19.6 mg, 0.04 mmol) was stirred at room temperature for 6 h, followed by the addition of [Cu(MeCN)<sub>4</sub>](PF<sub>6</sub>)<sub>2</sub> (14.6 mg, 0.04 mmol) and more stirring for 5 min. The resulting suspension was then filtered, and the filtrate was diffused with petroleum ether and Et<sub>2</sub>O (1:1). [Au<sub>2</sub>(2-bdppmapy)<sub>2</sub>](PF<sub>6</sub>)<sub>2</sub>·EtOH (**1**·EtOH) was isolated as colourless crystals after 2 days, which were collected, washed with Et<sub>2</sub>O, and dried in air. Yield for **1**: 76.7 mg (58% based on Au). Anal. Calcd for C<sub>62</sub>H<sub>56</sub>Au<sub>2</sub>F<sub>12</sub>N<sub>4</sub>P<sub>6</sub>: C, 44.73; H, 3.39; N, 3.37; found: C, 43.93; H, 3.70; N, 3.24 (%). IR (ATR, cm<sup>−1</sup>): 1591 (m), 1566 (w), 1476 (m), 1435 (s), 1283 (w), 1221 (m), 1159 (w), 1099 (m), 829 (vs), 775 (m), 733 (s), 691 (s). <sup>1</sup>H NMR (400 MHz, DMSO-*d*<sub>6</sub>, ppm):  $\delta$  8.06 (dd, *J* = 4.9, 1.3 Hz, 2H), 7.44–7.36 (m, 42 H), 6.75 (d, *J* = 8.6 Hz, 2H), 6.57 (dd, *J* = 6.9, 5.0 Hz, 2H), 4.22 (d, *J* = 2.4 Hz, 8H). <sup>13</sup>C NMR (101.6 MHz, DMSO-*d*<sub>6</sub>, ppm):  $\delta$  156.62, 147.20, 137.15, 136.97, 132.98, 132.89, 132.79, 128.93, 128.62, 128.59, 128.56, 112.12, 107.40, 49.82 ppm. <sup>31</sup>P{H} NMR (162 MHz, DMSO-*d*<sub>6</sub>, ppm):  $\delta$  44.66.

#### 3.3. Preparations of **1**—1 MPa, **1**—2.5 MPa, **1**—5 MPa, **1**—10 MPa, **1**—20 MPa, and **1g**

A mould ( $\Phi$  = 9 mm) containing 3 mg of **1** was subjected to pressures of 1 MPa, 2.5 MPa, 5 MPa, 10 MPa, and 20 MPa (hand press) for 10 min each. The pressure was then released and the pellets collected (**1**—1 MPa was collected as a powder due to the low pressure). Compound **1g** was prepared by grinding **1** (3 mg) in a mortar for more than 5 min.

#### 3.4. Preparations of **1r** and **1gr**

Samples of **1**-5 MPa and **1g** were placed in a small beaker (5 mL), and sealed with 5 mL of CH<sub>2</sub>Cl<sub>2</sub> in a 50 mL beaker for 5 min, respectively.

#### 3.5. Preparation of ‘Secret Writing Paper’

Powdered **1** (3 mg) was plastered onto a small filter paper ( $\Phi$  = 9 mm). This ‘secret writing paper’ was exposed to CH<sub>2</sub>Cl<sub>2</sub> vapor for 5 min to activate it before use.

#### 3.6. Single-Crystal X-Ray Diffraction (SCXRD) Determination

A single crystal of **1**·EtOH (0.30 mm  $\times$  0.30 mm  $\times$  0.10 mm) was selected directly from the synthesis. SCXRD measurements were performed on an Agilent Xcalibur diffractometer



(Agilent, Santa Clara, CA, USA) using Mo  $K\alpha$  ( $\lambda = 0.71073 \text{ \AA}$ ) radiation at 223 K. The diffraction data were collected and refined, and a multi-scan absorption correction was applied using CrysAlisPro 1.171.42.81a. The structure was solved by direct methods using SHELXS (Sheldrick, 2016/6) and refined by full-matrix least-squares methods against  $F^2$  using SHELXL (Sheldrick, 2016/6) [72]. The  $\text{PF}_6^-$  anion was disordered over two sites rotating along the F1-P3-F2 axis with occupancies of 0.50/0.50 for F3-F6/F3A-F6A. The EtOH mole was disordered at opposite positions with equal (0.5/0.5) occupancies. The disordered F atoms at the  $\text{PF}_6^-$  anion and the C and O atoms of the disordered EtOH molecule were refined isotropically, while all other non-hydrogen atoms were refined anisotropically. Hydrogen atoms were placed at calculated positions and constrained to ride over their parent C and N atoms. Selected crystallographic data and refinement parameters are listed in Table S1.

### 3.7. Computational Details

Theoretical calculations were conducted using the Gaussian 16-C01 software package at the B3LYP-GD3BJ/def2SVP level [73]. Based on the crystal structure, we froze the heavy atoms in the optimisation and optimised the hydrogen atoms.

## 4. Conclusions

In summary, we have synthesised a binuclear Au-P complex  $[\text{Au}_2(2\text{-bdppmapy})_2](\text{PF}_6)_2$  (**1**), which emitted yellow phosphorescence in the solid state at  $\lambda_{\text{max}} = 580 \text{ nm}$  upon 345 nm excitation. DFT calculations suggested that this PL is attributable to a combination of  $^3\text{LMCT}$  and  $^3\text{ILCT}$ . Induced by pressures as low as 2.5 MPa, the emission of **1** visibly shifted from yellow to green. The PXRD pattern changes indicated a clear phase transition, observable at 1 MPa and completed at pressures exceeding 5 MPa. This emission change could be recovered by exposure to  $\text{CH}_2\text{Cl}_2$  vapor, and these reversible transformations could be cycled multiple times. The mechanochromic PL behaviour of **1** was likely associated with the reducing of voids in the unit cell, which altered the inter- and intra-molecular  $\text{C-H}\cdots\pi$  interactions, perturbed electron densities over the  $-\text{PPh}_2$  and  $-\text{Py}$  groups, and varied energy gaps between the excited and ground states. Furthermore, a ‘secret writing paper’ impregnated with complex **1** was utilised to make invisible ink that can be seen under UV light and erased upon exposure to  $\text{CH}_2\text{Cl}_2$  vapor. This work presented an example of a novel recoverable mechanochromic PL material suitable for force-sensitive sensors. Additionally, our laboratory is actively exploring other stimuli-responsive photoluminescent complexes.

**Supplementary Materials:** The following supporting information can be downloaded at <https://www.mdpi.com/article/10.3390/molecules30092011/s1>, Figure S1: TGA curve of **1**; Figure S2: PXRD patterns of as-synthesised **1** and those simulated from the SCXRD data; Figure S3: IR spectra of **1** and **1**·EtOH; Figure S4:  $^1\text{H}$ ,  $^{13}\text{C}$ , and  $^{31}\text{P}\{^1\text{H}\}$  NMR spectra of **1** in  $\text{DMSO-}d_6$ ; Figure S5: Emission spectra and maximum wavelength of the emission spectra of **1** during the 5-round pressure-vapor cycles; Figure S6: Packing diagram indicating the void in **1**; Table S1: Selected crystallographic data and refinement parameters for **1**. Cartesian coordinates of molecule **1**.

**Author Contributions:** Z.-G.R. administrated the project, made the data curation, and wrote the original draft. N.Y., Y.C. and J.W. conducted formal analysis, investigation, and data curation. Y.L. performed the computational calculations. H.-X.L. undertook investigation and data curation. D.J.Y. reviewed data and edited the manuscript. All authors have read and agreed to the published version of the manuscript.

**Funding:** This work was financially supported by the National Natural Science Foundation of China (Grant No. 21671144).

**Institutional Review Board Statement:** Not applicable.

**Informed Consent Statement:** Not applicable.

**Data Availability Statement:** The crystallographic data are available from the Cambridge Crystallographic Data Centre (CCDC number 2419373). Other data not presented in the Supplementary Materials are available on request from the corresponding author.

**Conflicts of Interest:** The authors declare no conflicts of interest.

## References

1. Jin, M.; Ito, H. Solid-state luminescence of Au(I) complexes with external stimuli-responsive properties. *J. Photochem. Photobiol. C* **2022**, *51*, 100478. [\[CrossRef\]](#)
2. Tong, Y.; Chen, X.-W.; He, L.-H.; Chen, J.-L.; Liu, S.-J.; Wen, H.-R. Reversible stimuli-responsive luminescence of bimetallic cuprous complexes based on NH-deprotonated 3-(2'-pyridyl)pyrazole. *J. Mater. Chem. C* **2021**, *9*, 16664–16671. [\[CrossRef\]](#)
3. Yang, D.-D.; Xiao, T.; Yang, Y.-Y.; Xue, J.-H.; Shi, Y.-S.; Ma, Q.; Zheng, X.-J. Two viologen-based complexes as persistent luminescent materials and their applications in inkless print and anticounterfeiting. *Chem. Eng. J.* **2024**, *488*, 151047. [\[CrossRef\]](#)
4. Wei, Z.; Zhang, K.; Kim, C.K.; Tan, S.; Wang, S.; Wang, L.; Li, J.; Wang, Y. Stimuli-responsive cyclometalated platinum complex bearing bent molecular geometry for highly efficient solution-processable OLEDs. *Chin. Chem. Lett.* **2021**, *32*, 493–496. [\[CrossRef\]](#)
5. Takeda, H.; Kobayashi, A.; Tsuge, K. Recent developments of photoactive Cu(I) and Ag(I) complexes with diphosphine and related ligands. *Coord. Chem. Rev.* **2022**, *470*, 214700. [\[CrossRef\]](#)
6. Kumar, P.; Kaushik, R.; Ghosh, A.; Jose, D.A. Detection of Moisture by Fluorescent OFF-ON Sensor in Organic Solvents and Raw Food Products. *Anal. Chem.* **2016**, *88*, 11314–11318. [\[CrossRef\]](#)
7. Lv, C.-L.; Yang, C.-H.; Liu, L.-Y.; Zhang, Z.-C. Organoimido functionalized trinuclear gold(I) clusters with fluorescent chromophore. *Rare Met.* **2020**, *40*, 1437–1442. [\[CrossRef\]](#)
8. Lee, L.C.; Lo, K.K. Shining New Light on Biological Systems: Luminescent Transition Metal Complexes for Bioimaging and Biosensing Applications. *Chem. Rev.* **2024**, *124*, 8825–9014. [\[CrossRef\]](#)
9. Seki, T.; Takamatsu, Y.; Ito, H. A Screening Approach for the Discovery of Mechanochromic Gold(I) Isocyanide Complexes with Crystal-to-Crystal Phase Transitions. *J. Am. Chem. Soc.* **2016**, *138*, 6252–6260. [\[CrossRef\]](#)
10. Qin, Y.; She, P.; Huang, X.; Huang, W.; Zhao, Q. Luminescent manganese(II) complexes: Synthesis, properties and optoelectronic applications. *Coord. Chem. Rev.* **2020**, *416*, 213331. [\[CrossRef\]](#)
11. Li, Y.; Chen, L.; Ai, Y.; Hong, E.Y.; Chan, A.K.; Yam, V.W. Supramolecular Self-Assembly and Dual-Switch Vapochromic, Vapoluminescent, and Resistive Memory Behaviors of Amphiphilic Platinum(II) Complexes. *J. Am. Chem. Soc.* **2017**, *139*, 13858–13866. [\[CrossRef\]](#) [\[PubMed\]](#)
12. Gao, M.; Li, J.; Peng, N.; Jiang, L.; Zhao, S.; Fu, D.-Y.; Li, G. Multi-stimuli responsive lanthanides-based luminescent hydrogels for advanced information encryption. *J. Mol. Liq.* **2022**, *368*, 120681. [\[CrossRef\]](#)
13. Xiao, Z.-M.; Yang, J.-X.; Chen, X.; Tang, W.-J.; Peng, S.-K.; Hao, D.-B.; Zhao, Z.-P.; Zheng, J.; Li, D. A fluorescence–phosphorescence dual-emissive Cu<sub>3</sub>(pyrazolate)<sub>3</sub> complex with highly tunable emission colours for anticounterfeiting and temperature sensing. *Inorg. Chem. Front.* **2024**, *11*, 1808–1818. [\[CrossRef\]](#)
14. Yang, H.; Peng, S.K.; Zheng, J.; Luo, D.; Xie, M.; Huang, Y.L.; Cai, X.; Wang, J.; Zhou, X.P.; Li, D. Achiral Au(I) Cyclic Trinuclear Complexes with High-Efficiency Circularly Polarized Near-Infrared TADF. *Angew. Chem. Int. Ed.* **2023**, *62*, e202310495. [\[CrossRef\]](#)
15. Wu, N.M.; Ng, M.; Yam, V.W. Photochromic Benzo[b]phosphole Alkynylgold(I) Complexes with Mechanochromic Property to Serve as Multistimuli-Responsive Materials. *Angew. Chem. Int. Ed.* **2019**, *58*, 3027–3031. [\[CrossRef\]](#)
16. Wu, N.M.; Ng, M.; Yam, V.W. Photocontrolled multiple-state photochromic benzo[b]phosphole thieno[3,2-b]phosphole-containing alkynylgold(I) complex via selective light irradiation. *Nat. Commun.* **2022**, *13*, 33. [\[CrossRef\]](#)
17. Rolz, M.; Butschke, B.; Breit, B. Azobenzene-Integrated NHC Ligands: A Versatile Platform for Visible-Light-Switchable Metal Catalysis. *J. Am. Chem. Soc.* **2024**, *146*, 13210–13225. [\[CrossRef\]](#)
18. Pi, Q.; Bi, D.; Qiu, D.; Wang, H.; Cheng, X.; Feng, Y.; Zhao, Q.; Zhou, M. A dual-wavelength electrochromic film based on a Pt(II) complex for optical modulation at telecommunication wavelengths and dark solid-state display devices. *J. Mater. Chem. C* **2021**, *9*, 8994–9000. [\[CrossRef\]](#)
19. Banasz, R.; Wałęsa-Chorab, M. Polymeric complexes of transition metal ions as electrochromic materials: Synthesis and properties. *Coord. Chem. Rev.* **2019**, *389*, 1–18. [\[CrossRef\]](#)
20. Sun, N.; Zhang, S.T.; Simon, F.; Steiner, A.M.; Schubert, J.; Du, Y.; Qiao, Z.; Fery, A.; Lissel, F. Poly(3-hexylthiophene)s Functionalized with N-Heterocyclic Carbenes as Robust and Conductive Ligands for the Stabilization of Gold Nanoparticles. *Angew. Chem. Int. Ed.* **2021**, *60*, 3912–3917. [\[CrossRef\]](#)
21. Brown, C.M.; Carta, V.; Wolf, M.O. Thermochromic Solid-State Emission of Dipyridyl Sulfoxide Cu(I) Complexes. *Chem. Mater.* **2018**, *30*, 5786–5795. [\[CrossRef\]](#)

22. Artem'ev, A.V.; Ryzhikov, M.R.; Berezin, A.S.; Kolesnikov, I.E.; Samsonenko, D.G.; Bagryanskaya, I.Y. Photoluminescence of Ag(I) complexes with a square-planar coordination geometry: The first observation. *Inorg. Chem. Front.* **2019**, *6*, 2855–2864. [\[CrossRef\]](#)
23. Stal, S.; Huitorel, B.; Coustham, T.; Stephant, N.; Massuyeau, F.; Gacoin, T.; Bouteiller, L.; Perruchas, S. Photoactive CuI-Cross-Linked Polyurethane Materials. *ACS Appl. Mater. Interfaces* **2022**, *14*, 47931–47940. [\[CrossRef\]](#)
24. Artem'ev, A.V.; Rogovoy, M.I.; Odud, I.M.; Davydova, M.P.; Rakhmanova, M.I.; Petrov, P.A.; Brel, V.K.; Artushin, O.I.; Brylev, K.A.; Samsonenko, D.G.; et al. Toward highly efficient TADF-active Cu(I), Ag(I) and Au(I) carbene complexes using symmetry-based design strategy. *Inorg. Chem. Front.* **2024**, *11*, 8778–8788. [\[CrossRef\]](#)
25. Soto, M.A.; Carta, V.; Andrews, R.J.; Chaudhry, M.T.; MacLachlan, M.J. Structural Elucidation of Selective Solvatochromism in a Responsive-at-Metal Cyclometalated Platinum(II) Complex. *Angew. Chem. Int. Ed.* **2020**, *59*, 10348–10352. [\[CrossRef\]](#)
26. Nagy, M.; Rácz, D.; Nagy, Z.L.; Fehér, P.P.; Kalmár, J.; Fábíán, I.; Kiss, A.; Zsuga, M.; Kéki, S. Solvatochromic isocyanonaphthalene dyes as ligands for silver(I) complexes, their applicability in silver(I) detection and background reduction in biolabelling. *Sens. Actuators B* **2018**, *255*, 2555–2567. [\[CrossRef\]](#)
27. Seki, T.; Ozaki, T.; Okura, T.; Asakura, K.; Sakon, A.; Uekusa, H.; Ito, H. Interconvertible multiple photoluminescence color of a gold(I) isocyanide complex in the solid state: Solvent-induced blue-shifted and mechano-responsive red-shifted photoluminescence. *Chem. Sci.* **2015**, *6*, 2187–2195. [\[CrossRef\]](#)
28. Zhao, X.; Gong, J.; Li, Z.; Sung, H.H.Y.; Williams, I.D.; Lam, J.W.Y.; Zhao, Z.; Tang, B.Z.; Wong, W.Y.; Xu, L. Au...I coinage bonds: Boosting photoluminescence efficiency and solid-state molecular motion. *Aggregate* **2024**, *6*, e686. [\[CrossRef\]](#)
29. Li, H.; Yang, J.; Wang, Q.; Tong, H.; Zhu, J.; Liu, W.; Ouyang, G. Ligand Detachment—New Insight into the Mechanochromic Luminescence Mechanism of Copper Iodide Complexes with Thermally Activated Delayed Fluorescence. *Adv. Opt. Mater.* **2024**, *12*, 2400364. [\[CrossRef\]](#)
30. Chen, X.-W.; He, L.-H.; Ju, P.; Chen, J.-L.; Liu, S.-J.; Wen, H.-R. Mechanochromic luminescent materials of bimetallic Cu(I) complexes showing thermally activated delayed fluorescence. *J. Mater. Chem. C* **2020**, *8*, 16160–16167. [\[CrossRef\]](#)
31. Hashimoto, Y.; Katagiri, Y.; Tanaka, Y.; Yoshizawa, M. Solution-state mechanochromic luminescence of Pt(II)-complexes displayed within micellar aromatic capsules. *Chem. Sci.* **2023**, *14*, 14211–14216. [\[CrossRef\]](#) [\[PubMed\]](#)
32. Kwon, E.; Kim, J.; Lee, K.Y.; Kim, T.H. Non-Phase-Transition Luminescence Mechanochromism of a Copper(I) Coordination Polymer. *Inorg. Chem.* **2017**, *56*, 943–949. [\[CrossRef\]](#) [\[PubMed\]](#)
33. Deak, A.; Jobbagy, C.; Demeter, A.; Celko, L.; Cihlar, J.; Szabo, P.T.; Abranyi-Balogh, P.; Crawford, D.E.; Virieux, D.; Colacino, E. Mechanochemical synthesis of mononuclear gold(I) halide complexes of diphosphine ligands with tuneable luminescent properties. *Dalton Trans.* **2021**, *50*, 13337–13344. [\[CrossRef\]](#)
34. Seki, T.; Sakurada, K.; Ito, H. Controlling mechano- and seeding-triggered single-crystal-to-single-crystal phase transition: Molecular domino with a disconnection of aurophilic bonds. *Angew. Chem. Int. Ed. Engl.* **2013**, *52*, 12828–12832. [\[CrossRef\]](#)
35. Ito, H.; Muromoto, M.; Kurenuma, S.; Ishizaka, S.; Kitamura, N.; Sato, H.; Seki, T. Mechanical stimulation and solid seeding trigger single-crystal-to-single-crystal molecular domino transformations. *Nat. Commun.* **2013**, *4*, 2009. [\[CrossRef\]](#)
36. Zhang, X.; Wang, J.Y.; Ni, J.; Zhang, L.Y.; Chen, Z.N. Vapochromic and mechanochromic phosphorescence materials based on a platinum(II) complex with 4-trifluoromethylphenylacetylide. *Inorg. Chem.* **2012**, *51*, 5569–5579. [\[CrossRef\]](#)
37. Eddingsaas, N.; Suslick, K. Intense Mechanoluminescence and Gas Phase Reactions from the Sonication of an Organic Slurry. *J. Am. Chem. Soc.* **2007**, *129*, 6718–6719. [\[CrossRef\]](#)
38. Zhang, X.; Chi, Z.; Zhang, Y.; Liu, S.; Xu, J. Recent advances in mechanochromic luminescent metal complexes. *J. Mater. Chem. C* **2013**, *1*, 3376–3390. [\[CrossRef\]](#)
39. Cheng, S.; Chen, Z.; Yin, Y.; Sun, Y.; Liu, S. Progress in mechanochromic luminescence of gold(I) complexes. *Chin. Chem. Lett.* **2021**, *32*, 3718–3732. [\[CrossRef\]](#)
40. Chen, W.-T.; Li, C.-H.; Liang, Z.-Y.; Zhang, Z.-L.; Liu, D.-Q.; Ye, J.-W.; Chen, L.; Chen, X.-M. Large and Tunable Wavelength Blue Shifts in Luminescent Piezochromism of Cu(I) Complexes via a Guest Encapsulation Strategy. *ACS Mater. Lett.* **2024**, *6*, 2077–2084. [\[CrossRef\]](#)
41. Walters, D.T.; Aghakhanpour, R.B.; Powers, X.B.; Ghiassi, K.B.; Olmstead, M.M.; Balch, A.L. Utilization of a Nonemissive Triphosphine Ligand to Construct a Luminescent Gold(I)-Box That Undergoes Mechanochromic Collapse into a Helical Complex. *J. Am. Chem. Soc.* **2018**, *140*, 7533–7542. [\[CrossRef\]](#) [\[PubMed\]](#)
42. Li, W.-B.; Luo, W.-J.; Li, K.-X.; Yuan, W.-Z.; Zhang, Y.-M. Aggregation-induced phosphorescence and mechanochromic luminescence of a tetraphenylethene-based gold(I) isocyanide complex. *Chin. Chem. Lett.* **2017**, *28*, 1300–1305. [\[CrossRef\]](#)
43. Zhang, X.; Zhang, L.-Y.; Wang, J.-Y.; Dai, F.-R.; Chen, Z.-N. Two-step phosphorescent mechanochromism due to intramolecular deformation. *J. Mater. Chem. C* **2020**, *8*, 715–720. [\[CrossRef\]](#)
44. Zhang, J.; He, B.; Wu, W.; Alam, P.; Zhang, H.; Gong, J.; Song, F.; Wang, Z.; Sung, H.H.Y.; Williams, I.D.; et al. Molecular Motions in AIEgen Crystals: Turning on Photoluminescence by Force-Induced Filament Sliding. *J. Am. Chem. Soc.* **2020**, *142*, 14608–14618. [\[CrossRef\]](#)

45. Ai, Y.; Li, Y.; Chan, M.H.; Xiao, G.; Zou, B.; Yam, V.W. Realization of Distinct Mechano- and Piezochromic Behaviors via Alkoxy Chain Length-Modulated Phosphorescent Properties and Multidimensional Self-Assembly Structures of Dinuclear Platinum(II) Complexes. *J. Am. Chem. Soc.* **2021**, *143*, 10659–10667. [\[CrossRef\]](#)
46. Balch, A.L. Dynamic crystals: Visually detected mechanochemical changes in the luminescence of gold and other transition-metal complexes. *Angew. Chem. Int. Ed. Engl.* **2009**, *48*, 2641–2644. [\[CrossRef\]](#)
47. Kuchison, A.M.; Wolf, M.O.; Patrick, B.O. Conjugated ligand-based tribochromic luminescence. *Chem. Commun.* **2009**, *47*, 7387–7389. [\[CrossRef\]](#)
48. Lechner, A.; Gliemann, G. Pressure Effects on the Absorption and Emission of Tetracyanoplatinates(II) in Solution. *J. Am. Chem. Soc.* **1989**, *111*, 7469–7475. [\[CrossRef\]](#)
49. Theoretical Studies of the Spectroscopic Properties of  $[\text{Pt}(\text{trpy})\text{C}:\text{CR}]^+$  ( $\text{trpy} = 2,2',6',2''\text{-Terpyridine}$ ;  $\text{R} = \text{H}$ ,  $\text{CH}_2\text{OH}$ , and  $\text{C}_6\text{H}_5$ ). *J. Phys. Chem. A* **2005**, *109*, 8809–8818. [\[CrossRef\]](#)
50. Grey, J.K.; Butler, I.S.; Reber, C. Pressure-Induced Enhancements of Luminescence Intensities and Lifetimes Correlated with Emitting-State Distortions for Thiocyanate and Selenocyanate Complexes of Platinum(II) and Palladium(II). *Inorg. Chem.* **2003**, *42*, 6503–6518. [\[CrossRef\]](#)
51. Rawashdeh-Omary, M.A.; Omary, M.A.; Patterson, H.H.; Fackler, J.P. Excited-State Interactions for  $[\text{Au}(\text{CN})_2^-]_n$  and  $[\text{Ag}(\text{CN})_2^-]_n$  Oligomers in Solution. Formation of Luminescent Gold-Gold Bonded Excimers and Exciplexes. *J. Am. Chem. Soc.* **2001**, *123*, 11237–11247. [\[CrossRef\]](#) [\[PubMed\]](#)
52. Seki, T.; Tokodai, N.; Omagari, S.; Nakanishi, T.; Hasegawa, Y.; Iwasa, T.; Taketsugu, T.; Ito, H. Luminescent Mechanochromic 9-Anthryl Gold(I) Isocyanide Complex with an Emission Maximum at 900 nm after Mechanical Stimulation. *J. Am. Chem. Soc.* **2017**, *139*, 6514–6517. [\[CrossRef\]](#) [\[PubMed\]](#)
53. Xie, M.; Chen, X.R.; Wu, K.; Lu, Z.; Wang, K.; Li, N.; Wei, R.J.; Zhan, S.Z.; Ning, G.H.; Zou, B.; et al. Pressure-induced phosphorescence enhancement and piezochromism of a carbazole-based cyclic trinuclear Cu(I) complex. *Chem. Sci.* **2021**, *12*, 4425–4431. [\[CrossRef\]](#) [\[PubMed\]](#)
54. Zhang, Y.; Ni, J.; Zhu, Y.; Zeng, Q.; Ai, Y.; Li, Y. Multi-stimuli responsive Pt(II) complexes for information storage and anti-counterfeiting. *Chem. Eng. J.* **2024**, *498*, 155049. [\[CrossRef\]](#)
55. Ono, T.; Tsukiyama, Y.; Taema, A.; Sato, H.; Kiyooka, H.; Yamaguchi, Y.; Nagahashi, A.; Nishiyama, M.; Akahama, Y.; Ozawa, Y.; et al. Piezofluorochromism in Charge-Transfer Inclusion Crystals: The Influence of High Pressure versus Mechanical Grinding. *ChemPhotoChem.* **2018**, *2*, 416–420. [\[CrossRef\]](#)
56. Ito, H.; Saito, T.; Oshima, N.; Kitamura, N.; Ishizaka, S.; Hinatsu, Y.; Wakeshima, M.; Kato, M.; Tsuge, K.; Sawamura, M. Reversible Mechanochromic Luminescence of  $[(\text{C}_6\text{F}_5\text{Au})_2(\mu\text{-}1,4\text{-Diisocyanobenzene})]$ . *J. Am. Chem. Soc.* **2008**, *130*, 10044–10045. [\[CrossRef\]](#)
57. Lim, S.H.; Olmstead, M.M.; Balch, A.L. Molecular accordion: Vapoluminescence and molecular flexibility in the orange and green luminescent crystals of the dimer,  $\text{Au}_2(\mu\text{-bis}(\text{diphenylphosphino})\text{ethane})_2\text{Br}_2$ . *J. Am. Chem. Soc.* **2011**, *133*, 10229–10238. [\[CrossRef\]](#)
58. Lim, S.H.; Olmstead, M.M.; Balch, A.L. Inorganic topochemistry. Vapor-induced solid state transformations of luminescent, three-coordinate gold(I) complexes. *Chem. Sci.* **2013**, *4*, 311–318. [\[CrossRef\]](#)
59. Deák, A.; Jobbagy, C.; Marsi, G.; Molnar, M.; Szakacs, Z.; Baranyai, P. Anion-, Solvent-, Temperature-, and Mechano-Responsive Photoluminescence in Gold(I) Diphosphine-Based Dimers. *Chem. Eur. J.* **2015**, *21*, 11495–11508. [\[CrossRef\]](#)
60. Jobbágy, C.; Baranyai, P.; Marsi, G.; Rácz, B.; Li, L.; Naumov, P.; Deák, A. Novel gold(I) diphosphine-based dimers with aurophilicity triggered multistimuli light-emitting properties. *J. Mater. Chem. C* **2016**, *4*, 10253–10264. [\[CrossRef\]](#)
61. Hu, S.; Yan, S.; Hu, Y.; Young, D.J.; Li, H.-X.; Lu, C.; He, J.-H.; Ren, Z.-G. A PN(Pz)P ligand protected  $\text{Au}_2\text{Cu}_2$  complex for photoluminescent ultra-low humidity detection with reversible single-crystal-to-single-crystal transformations. *Inorg. Chem. Front.* **2023**, *10*, 3706–3713. [\[CrossRef\]](#)
62. Huang, J.; Hu, Y.; Xu, W.; Yang, W.; Lu, C.; Young, D.J.; Ren, Z.-G. Switchable Fluorescence of a Mechanical Stimulus-Responsive Au-P-S Complex. *Molecules* **2024**, *29*, 5736. [\[CrossRef\]](#) [\[PubMed\]](#)
63. Cui, L.; Zhang, J.; Yan, S.; Yang, N.; Young, D.J.; Li, H.-X.; He, X.; Lu, Y.; Ren, Z.-G. A phosphorescent Au-P complex exhibiting ROS generation, enhanced emission in polymers and photodynamic inactivation of bacteria activities. *J. Mol. Struct.* **2025**, *1337*, 142254. [\[CrossRef\]](#)
64. Pal, S.; Kathewad, N.; Pant, R.; Khan, S. Synthesis, Characterization, and Luminescence Studies of Gold(I) Complexes with PNP- and PNB-Based Ligand Systems. *Inorg. Chem.* **2015**, *54*, 10172–10183. [\[CrossRef\]](#)
65. Kathewad, N.; Kumar, N.; Dasgupta, R.; Ghosh, M.; Pal, S.; Khan, S. The syntheses and photophysical properties of PNP-based Au(I) complexes with strong intramolecular  $\text{Au} \cdots \text{Au}$  interactions. *Dalton Trans.* **2019**, *48*, 7274–7280. [\[CrossRef\]](#)
66. Sathyanarayana, A.; Nakamura, S.-Y.; Hisano, K.; Tsutsumi, O.; Srinivas, K.; Prabusankar, G. Controlling the solid-state luminescence of gold(I) N-heterocyclic carbene complexes through changes in the structure of molecular aggregates. *Sci. China Chem.* **2018**, *61*, 957–965. [\[CrossRef\]](#)

67. Wang, X.-Y.; Zhang, J.; Dong, Y.-B.; Zhang, Y.; Yin, J.; Liu, S.H. Different structures modulated mechanochromism and aggregation-induced emission in a series of Gold(I) complexes. *Dye. Pigment.* **2018**, *156*, 74–81. [[CrossRef](#)]
68. Chen, Z.; Liu, G.; Pu, S.; Liu, S.H. Bipyridine-based aggregation-induced phosphorescent emission (AIPE)-active gold(I) complex with reversible phosphorescent mechanochromism and self-assembly characteristics. *Dye. Pigment.* **2018**, *152*, 54–59. [[CrossRef](#)]
69. Lu, T.; Chen, F. Multiwfn: A multifunctional wavefunction analyzer. *J. Comput. Chem.* **2012**, *33*, 580–592. [[CrossRef](#)]
70. Tang, W.-J.; Yang, H.; Peng, S.-K.; Xiao, Z.-M.; Huang, G.-Q.; Zheng, J.; Li, D. Multistimuli-responsive behavior of a phosphorescent Cu<sub>3</sub>pyrazolate<sub>3</sub> complex for luminescent logic gates and encrypted information transformation. *Inorg. Chem. Front.* **2023**, *10*, 2594–2606. [[CrossRef](#)]
71. Zhang, J.-F.; Xin, G.; Fu, W.-F.; Xu, H.; Li, L. Interaction of free functional group with platinum(II) center in cyclometalated complexes: A structural and photophysical property investigation. *Inorganica Chim. Acta* **2010**, *363*, 338–345. [[CrossRef](#)]
72. Sheldrick, G.M. *SHELXTL-2016*; Universität Göttingen: Göttingen, Germany, 2016.
73. Frisch, M.J.; Trucks, G.W.; Schlegel, H.B.; Scuseria, G.E.; Robb, M.A.; Cheeseman, J.R.; Scalmani, G.; Barone, V.; Petersson, G.A.; Nakatsuji, H.; et al. *Gaussian 16 Rev. C.01*; Gaussian, Inc.: Wallingford, CT, USA, 2016.

**Disclaimer/Publisher’s Note:** The statements, opinions and data contained in all publications are solely those of the individual author(s) and contributor(s) and not of MDPI and/or the editor(s). MDPI and/or the editor(s) disclaim responsibility for any injury to people or property resulting from any ideas, methods, instructions or products referred to in the content.